Excellent Balance of Ultimate Tensile Strength and Ductility in a Ti–6Al–2Sn–4Zr–2Mo–Si Alloy Having Duplex $\alpha + \alpha$' Microstructure: Effect of Microstructural Factors from Experimental Study and Machine Learning

Irvin Séchepée, Paul Paulain, Yuka Nagasaki, Riku Tanaka, Hiroaki Matsumoto, Vincent Velay

Excellent Balance of Ultimate Tensile Strength and Ductility in a Ti–6Al–2Sn–4Zr–2Mo–Si Alloy Having Duplex $\alpha + \alpha'$ Microstructure: Effect of Microstructural Factors from Experimental Study and Machine Learning

Irvin Séchepée[1,*1], Paul Paulain[1,2], Yuka Nagasaki[1,*1], Riku Tanaka[1,*1], Hiroaki Matsumoto[1,*2] and Vincent Velay[3]

[1]*Department of Advanced Materials Science, Faculty of Engineering, Kagawa University, 2217-20 Hayashi-cho, Takamatsu 761-0396, Japan*
[2]*Université de technologie de Compiègne, Rue du Docteur Schweitzer CS 60319 60203 Compiègne – France*
[3]*Université de Toulouse, CNRS Mines Albi, INSA, ISAE, ICA (Institut Clément Ader), Campus Jarlard - 81013 ALBI Cedex 09 – France*

This research focuses on the systematic study of a Ti–6Al–2Sn–4Zr–2Mo–Si titanium alloy and the characterization of $\alpha + \beta$ (equiaxed and bimodal) and $\alpha + \alpha'$ (duplex) microstructures. It provides more insights on the outstanding advantages of the duplex ($\alpha + \alpha'$) microstructure, especially on its exceptional work hardening and strength-ductility balance. The heat treatment conditions required to form equiaxed, bimodal and duplex microstructures and their effects on the grain size and the phase proportion are discussed. It shows how the microstructural parameters can be controlled thanks to the heat treatment temperatures, the holding times and possible aging processes. The influence of such microstructural factors on the tensile properties of each alloy is investigated, especially on strength (proof stress, ultimate tensile strength), ductility (plastic elongation) and work hardening properties. The duplex ($\alpha + \alpha'$) microstructure is compared with the equiaxed and bimodal microstructures and its advantages are displayed, highlighting the better strength-ductility balance and superior work hardening properties of the duplex microstructure. Indeed, the deformed microstructure of the duplex ($\alpha + \alpha'$) microstructure reveals more homogeneous strain partitioning than that of the bimodal ($\alpha + \beta$) microstructure. Thus, this work proved the potential of an optimized duplex ($\alpha + \alpha'$) microstructure for the enhanced tensile properties at room temperature. Finally, a machine learning model using gradient boosting regression trees is used to quantify the importance of the microstructural factors (type of microstructure, grain size and phase ratio) on the mechanical properties.

1. Introduction

Titanium alloys are high-performance materials that are used for their exceptional characteristics, especially corrosion resistance, high-temperature functioning and great strength to weight ratio.[1–3] They are key materials for critical parts in many sectors such as the aerospace, biomedical and defense industries. Various researches have been done on them in order to study their properties.[1,3] The Ti–6Al–4V (Ti-64) alloy is one of the most used titanium alloys in the industry for its extraordinary balance between its properties.[4–6] Additionally, thanks to its enhanced high-temperature performance, the Ti–6Al–2Sn–4Zr–2Mo–Si (Ti-6242S) alloy is used to replace the Ti-64 alloy.[7] However, compared to other metals like steels, the work hardening properties of titanium alloys are relatively low.[8] Increasing the work hardening[9] (while keeping high strength and high ductility) would allow to improve the homogeneous deformation behavior, toughness, damage tolerance and energy absorption ability of such titanium alloys[10] and promote their usage.

Indeed, thermo-mechanical processing is usually used to produce the different microstructures of titanium alloys and get the mechanical properties desired. The control of the process conditions like the heat treatment temperatures or the holding times allows managing the quality of the microstructure (i.e. the grain sizes and phase proportions).[11–13] Such microstructural factors are known to influence the mechanical properties.[12,14] The Hall-Petch effect is one of the most famous relationships that links the microstructural parameters on a micro scale to the mechanical properties on a macro scale (in this case, the grain size to the strength of the material).[15–17] For the ($\alpha + \beta$) Ti alloys, a microstructural control technique based on equilibrium phases (α and β phases) for the enhanced mechanical properties has been established.[18] In this work, we focus on the Ti-6242S alloy and aim at further enhancement of the mechanical properties and their balance with a new type of microstructural control based on a non-equilibrium phase (α' martensite (with HCP structure)).

The mechanical properties of the α' martensite alone are very poor in this kind of titanium alloy. As a consequence, the martensite is usually avoided or intentionally decomposed back into β phase[19,20] for microstructural control in practical applications. However, when coupled with α phase, the $\alpha + \alpha'$ microstructure displays exceptional mechanical properties. Previous researches on Ti–6Al–4V show that such $\alpha + \alpha'$ duplex microstructure exhibits improved strength and ductility properties[10,21–23] with a remarkable work hardening ability obtained by controlling the α and α' proportions through managing the annealing temperature. In detail, the present authors have previously presented for the Ti-64 alloy that the origin of high ductility in the $\alpha + \alpha'$ microstructure (duplex ($\alpha + \alpha'$) microstructure) was attributed to a frequent occurrence of $\{10\bar{1}1\}$ twinning and its easier motion (thanks to V-enrichment in the retained β phase before α' martensite transformation).[21] In addition, Dumas *et al.*, quite recently have reported for the Ti-64 alloy that the

*[1]Graduate Student, Kagawa University
*[2]Corresponding author, E-mail: matsumoto.hiroaki@kagawa-u.ac.jp

cluster of three α'-variants with the inter-variant boundary of $\{13\bar{4}1\}$ type twin formed in duplex ($\alpha + \alpha'$) microstructure contributed to high ductility by reorientation of $\{13\bar{4}1\}$ twinned boundary.[10] Therefore, the Ti alloys having an optimum $\alpha + \alpha'$ microstructure are expected to enhance the strength - ductility balance and work hardening behavior more than conventional ($\alpha + \beta$) microstructures. So far, there has been no systematic work on the effect of grain size and α' fraction on the strength, ductility and work hardening behavior in the duplex ($\alpha + \alpha'$) microstructure as compared to the case of conventional ($\alpha + \beta$) microstructures. In addition, there are no reports on the mechanical behavior of α'-martensite for the Ti-6242S alloy.

Designing titanium alloys is a complicated task as many factors such as chemical compositions, microstructure properties and process conditions can be considered. In spite of that, most of the relationships between these factors are nonlinear and not easy to process. Therefore, for the past years, the use of machine learning has gained in popularity in the field of materials science to understand better the complex relationships between microstructures and properties. Previous researches have shown interesting results on using such tools to model tensile and/or fatigue properties of titanium alloys thanks to whether their chemical composition[24] or their process conditions[25] or both of them.[26–29] Other investigations work with different perspectives as for examples using microstructural factors for the prediction of mechanical properties.[18,30] Alternatively, it is also possible to reverse the method and use mechanical properties to predict microstructures and/or processing conditions.[31] Nonetheless, machine learning can not only be used to predict such outcomes but also to measure the importances of the parameters during the prediction. For example, our previous work[18] showed that primary α fraction had great importance in modeling proof stress when considering ($\alpha + \beta$) lamellar, bimodal and equiaxed microstructures in the Ti–5Al–2Sn–2Zr–4Cr–4Mo (Ti-17) alloy. Similarly, results in Ref. 30) displayed that β fraction was dominant in predicting yield strength whereas grain size, strain rate and β fraction were almost equally important in modeling hardening for Ti–6Al–4V alloy.

This paper focuses on the systematic study of the Ti-6242S alloy and the characterization of the duplex ($\alpha + \alpha'$) microstructures comparing the equiaxed ($\alpha + \beta$) and bimodal ($\alpha + \beta$) microstructures. It provides more knowledge on the outstanding advantages of the duplex ($\alpha + \alpha'$) microstructure regarding its improved work hardening ability and strength-ductility balance. Here, we experimentally examined the effect of phase constituent, grain size, morphology and α/β or α/α' fractions on the mechanical behavior. Furthermore, we also carried out machine learning for linking microstructural factors and mechanical properties more quantitatively. Thus, this paper aims at clarifying the potential of ($\alpha + \alpha'$) microstructures in the Ti-6242S alloy for the enhanced mechanical properties at room temperature.

2. Experimental Procedures

2.1 Heat treatment processes

In this research, the titanium alloy Ti–6Al–2Sn–4Zr–2Mo–Si (Ti-6242S) is studied. The Ti-6242S alloy with a chemical composition (in mass%) of 6.1Al, 2.0Sn, 4.1Zr, 2.0Mo, 0.12Si, 0.1O, 0.02N, and balance Ti was used in this work. As-received plates with a thickness of 4 mm (W20 mm-L35 mm) were hot-rolled at 850°C (with holding time for 4 min) in order to get rolled plates having a thickness ranging from 1.3 to 1.4 mm. Different microstructures were produced regarding specific processes and the heat treatment temperatures were always below the β transus of 990°C. Using these hot rolled plates, three types (equiaxed ($\alpha + \beta$), bimodal ($\alpha + \beta$) and duplex ($\alpha + \alpha'$)) of microstructures were investigated. For making the equiaxed microstructure, we carried out annealing at temperatures of 800°C or 900°C and for several holding times from 30 minutes to 240 minutes followed by cooling (C), more specifically air cooling (AC) or furnace cooling (FC) (see Fig. 1(a)). A total of 11 different treatment conditions was used for the equiaxed microstructures. The bimodal microstructure is produced using the same process as for the equiaxed microstructure but followed by additional aging. Here, aging temperatures of 450°C, 550°C and 650°C were applied for a fixed holding time of 120 minutes followed by oil quenching (Q_o) (see Fig. 1(a)). Here, aging was carried out in an argon atmosphere. In this case, the aging process allows the formation of $\alpha + \beta$ lamellas inside the prior β grain. Here, 9 distinct bimodal microstructures were produced.

Finally, regarding the duplex microstructure consisting of primary α phase and α' martensite, the alloy is solution treated for temperatures between 850°C and 980°C for 15 minutes and then quenched into ice water (Q_w) in order to produce the α' martensitic phase (see Fig. 1(b)). Here, quenching is necessary to keep the metastable α' at room temperature (if not, the diffusion process activated during slow cooling would form ($\alpha + \beta$) phases instead of α'). For the duplex microstructures, we used 9 different treatment conditions.

2.2 Microstructure observations

The microstructures were observed with a JEOL JSM-7001F field emission gun scanning electron microscope (FE-SEM) fitted with an electron back-scattering diffraction (EBSD) analyzer equipped with the HKL Channel 5 software. And, the morphology of the α' martensite was also observed by a transmission electron microscope (TEM) (JEOL-JEM 2100F). The microstructural factors (grain sizes, phase ratios) were measured with the ImageJ software. A statistical approach was used to measure the average grain size for each microstructure. More precisely, we measured the surface areas of between 30 and 50 grains for each of the 2 or 3 SEM images for a minimum of 80 total grains per microstructure. We considered the average grain as a spherical inclusion (circular in 2D) and computed the equivalent average grain size thanks to $d_{eq} = 2\sqrt{S/\pi}$ with S the surface area in μm^2.

2.3 Tensile test

Mechanical properties (0.2% proof stress, ultimate tensile strength (UTS), elongation to fracture) were measured thanks to tensile tests. The tensile specimens (which surface was mechanically polished to avoid the thin oxidation layer

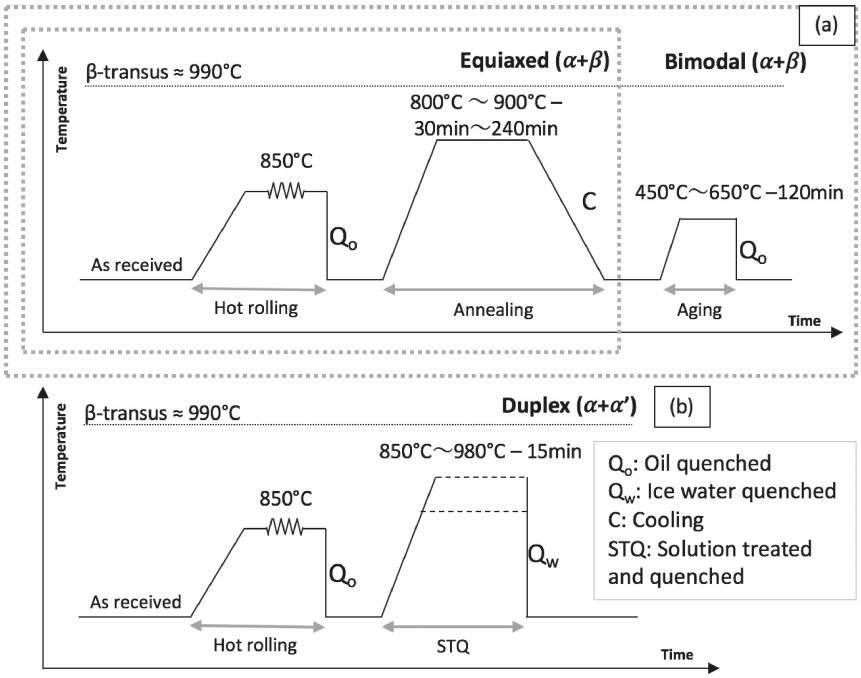

Fig. 1 Heat treatment processes for (a) equiaxed ($\alpha + \beta$) and bimodal ($\alpha + \beta$), and (b) duplex ($\alpha + \alpha'$) microstructures.

completely) had a gauge of 10.5 mm, a width of 2 mm for a thickness ranging from 1.0 to 1.2 mm and were produced so that the tensile direction would be parallel to the rolling direction (before heat treatment). The tensile tests were performed at room temperature, in air atmosphere and with an initial strain rate of $5 \times 10^{-4}\,s^{-1}$.

2.4 Machine learning

A numerical approach using machine learning was also implemented in order to understand better the impact of microstructural factors on mechanical properties. Thanks to the open-source scikit-learn library (v.0.24.1) of Python, a model of regression tree was used to predict the mechanical properties.

In order to understand the impacts of microstructural factors such as grain size, phase constituent and fraction of α/β or α/α' on tensile properties more quantitatively, we implemented a numerical approach using machine learning. The dataset in this research is composed of 37 sets of microstructural parameters and mechanical properties. With the 29 initial data (11 equiaxed, 9 bimodal, 9 duplex), 8 supplementary duplicates were added to the dataset for data size concern. These 8 duplicates consist of identical microstructural properties (grain size and phase ratio) but different mechanical properties for 4 of the duplex samples. In these cases, for 1 heat treatment condition, tensile testing was done 3 times, thus giving 3 slightly different set of mechanical properties (1 from initial data and 2 from duplicates) for 1 given microstructural set. In this regard, variation coefficients of 2.99%, 1.76%, 14.3% and 7.45% respectively for the proof stress, UTS, plastic elongation and work hardening exponent were observed for these duplicates. Therefore, the dataset of 37 sets is composed of 11 equiaxed, 9 bimodal and 17 duplex microstructures. Because the dataset is pretty small, algorithms such as neural networks could not be used. Indeed, this kind of heavy algorithm requires larger datasets in order to be effective. Therefore a less complex model such as regression tree was preferred.[32] Among regression tree models, the gradient boosting algorithm was chosen because of its better stability and precision.[33,34] The study of feature importance (using the permutation importance for less dependence between the parameters[35]) allowed the interpretation of how microstructural parameters influence the mechanical properties.

3. Results and Discussion

3.1 Experimental results

3.1.1 Typical microstructures

The $\alpha + \beta$ titanium alloy Ti-6242S having different microstructures is investigated in this study. Especially, we focus on the equiaxed ($\alpha + \beta$), bimodal ($\alpha + \beta$) and duplex ($\alpha + \alpha'$) microstructures. The first two are equilibrium microstructures whereas the duplex one is metastable. Heat treating the alloy at temperatures below the β transus (approximatively 990°C) allows the co-existence of two phases (α and β phases) inside the alloy. The main phase, which is the α phase has a hexagonal close-packed (HCP) structure and corresponds to the black phase on the SEM micrographs of this research (see Fig. 2(a)). The β phase has a body-centered cubic (BCC) crystal structure and corresponds to the white phase on the SEM images.

With respect to the equiaxed ($\alpha + \beta$) microstructure, typical equiaxed microstructures are displayed in Fig. 2(a). The equiaxed microstructure is characterized by its globular α grains whose size varies regarding the heat treatment conditions.[1,3] Here, we confirmed that the α grains grew coarser for longer holding times (static recrystallization process). In the present study, grain sizes can increase from 2.50 µm to 3.94 µm for a given treatment temperature (900°C). Additionally, changing the treatment temperature (800°C or 900°C) also reveals different grain sizes.[1,3] It is

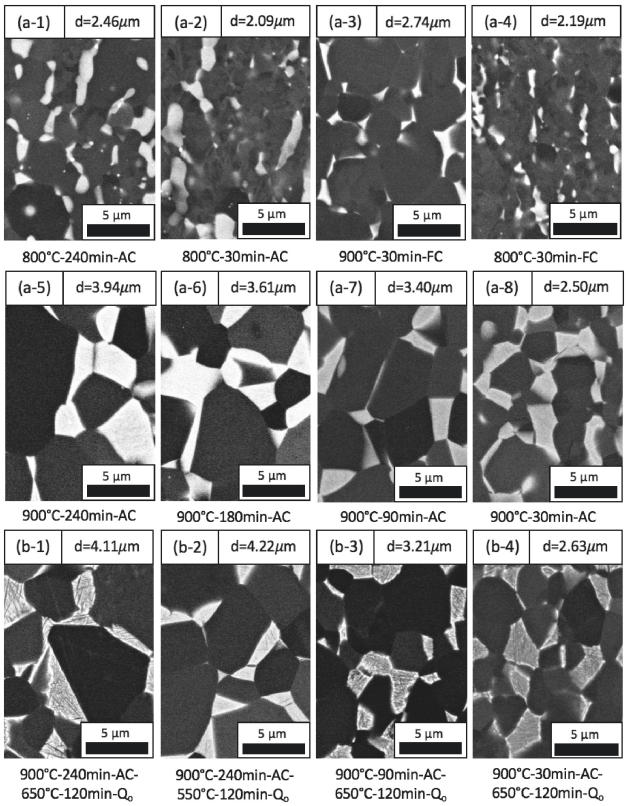

Fig. 2 SEM micrographs of the (a) equiaxed ($\alpha + \beta$) microstructure and (b) bimodal ($\alpha + \beta$) microstructure. Herein, heat treatment conditions are also depicted (d stands for grain size, AC for air cooling and Q_o for oil cooling).

noticeable that grain sizes at 800°C are finer than grain sizes at 900°C for the same holding time (respectively 2.46 µm versus 3.94 µm for 800°C-240 min and 900°C-240 min). On the other hand, phase proportions don't seem to vary much with increasing holding times (around 76% of α for each holding time at 900°C). However, changing the treatment temperature does change the amount of α and β.[1,3] Indeed, 76% of α phase was measured at 900°C while 87% of α was formed at 800°C. Overall, the equiaxed microstructure and its globular grains allow great ductility (elongation).[1,3,26] Controlling such microstructural factors is important as it impacts mechanical properties like strength or ductility.[1,3] Their influence will be further discussed later in part 3-2, on mechanical properties.

Additionally, typical bimodal microstructures are shown in Fig. 2(b). The aging process needed to produce bimodal microstructures allows the formation of α lamellas inside the prior β grains. The size (width) and the proportions of α lamellas inside the β grain also depend on the aging treatment conditions. The effect of the aging temperature can be observed on SEM micrographs (b-1) and (b-2) of Fig. 2(b), where 650°C aging temperature produces more α lamellas than aging at 550°C. However, it does not affect the grain size nor the primary α fraction which are mainly determined by the prior annealing treatment. In Fig. 2(b), we can compare the micrographs (b-1), (b-3) and (b-4) having different annealing holding times (respectively 240 min, 90 min and 30 min). It is noticeable that finer lamellas are produced for a prior annealing time of 240 min than for

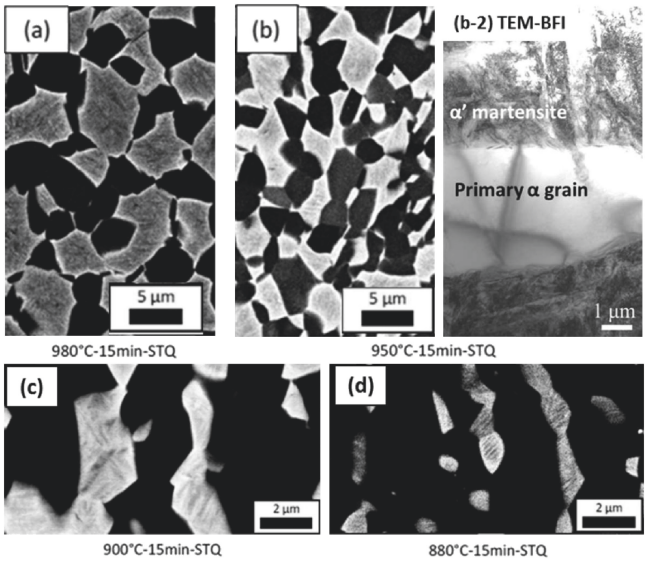

Fig. 3 SEM micrographs of the duplex ($\alpha + \alpha'$) microstructure. (a) 980°C-15 min-STQ (Solution treated and quenched), (b) 950°C-15 min-STQ, (c) 900°C-15 min-STQ, (d) 880°C-15 min-STQ. And (b-2) bright field TEM image on the 950°C-15 min-STQ sample.

90 min or 30 min. For bimodal microstructures, the formation of ($\alpha + \beta$) lamellas greatly improves strength while ductility may be deteriorated compared to equiaxed microstructure.[36,37] More information about the mechanical properties will be given afterward.

With respect to the duplex ($\alpha + \alpha'$) microstructure, several microstructures can be observed in Fig. 3 and are characterized by the formation of α' acicular martensite (with HCP structure) instead of β thanks to rapid cooling (quenching). From Fig. 3, white area corresponds to the region of aggregate of acicular α' martensite. The α' martensite alone usually promotes strengthening while lowering ductility.[38] However, in the duplex microstructure, the coexistence of α and α' allows great compatibilities at grain boundaries thanks to both phases having the same HCP crystal structure. Therefore an improvement in ductility properties can be observed. It has been studied that α' exhibits extraordinary work hardening and ductility properties in the case of the $\alpha + \alpha'$ duplex microstructure.[10,19–21] As for the morphology of the α' martensite, we can observe from the TEM image of Fig. 3(b-2) that fine acicular α' martensite is formed from parent β phase. Herein, a significant amount of the fringe-diffraction contrast could be observed in α' martensite, revealing the highly dense dislocations. As the typical characteristic of α' martensite, there are many $\{10\bar{1}1\}$ twins which are known to be formed during martensitic transformation of β/α' as an invariant deformation mode.[39] Similar to the equiaxed microstructure, the effect of heat treatment temperatures on phase proportions is observable in Fig. 3 where primary α fraction (black phase) increases while decreasing the temperature. Because of the short holding times (15 min), grain growth is also mainly influenced by the treatment temperatures.

Later on, grain sizes and phase proportions and their effects on the mechanical properties (strength, ductility, work hardening) of the duplex microstructure will be discussed.

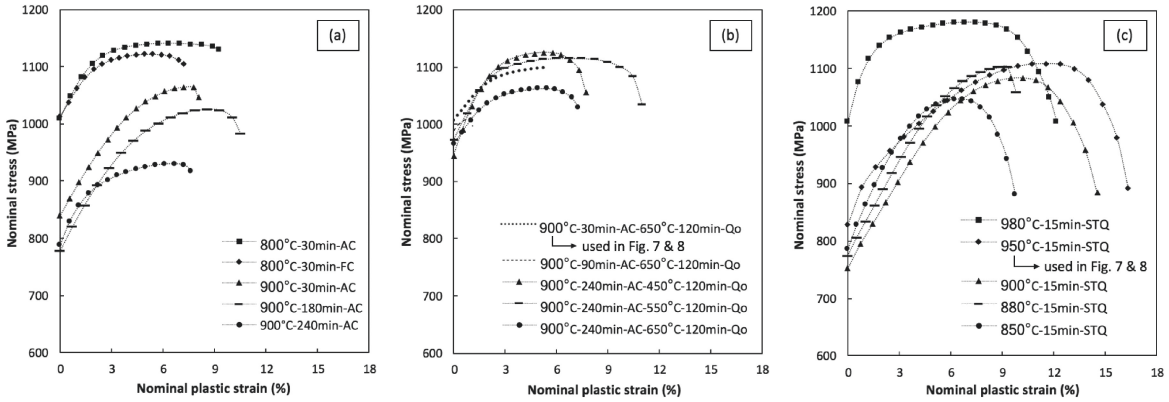

Fig. 4 Examples of nominal stress-plastic strain curves of (a) equiaxed ($\alpha + \beta$), (b) bimodal ($\alpha + \beta$), (c) duplex ($\alpha + \alpha'$) microstructures having different treatment conditions.

3.1.2 Tensile properties

Mechanical properties such as proof stress, ultimate tensile strength, plastic elongation and work hardening at room temperature were determined for each microstructure using uniaxial tensile tests performed alongside the rolling direction (Fig. 4). The influence of grain sizes and phase proportions on these mechanical properties were also studied (Fig. 5).

As for the case of equiaxed ($\alpha + \beta$) microstructure, Fig. 4(a) shows the strain-plastic stress curves for some of them among a total of 11 different treatment conditions taken into account in this study. We can note that two groups of properties were highlighted. The samples heat treated at 900°C for different holding times (from 30 min to 240 min) displayed high work hardening properties while having medium strength (Fig. 4(a)). Such properties were related to high β proportions (around 24%) and bigger grain sizes (from 2.5 to 4.0 µm). On the other hand, the samples produced by heating at 800°C and the ones with furnace cooling (a slower cooling than air cooling) revealed lower work hardening abilities but higher strength than its analogous 900°C microstructures. Such properties were related to lower β proportions (around 12%) and smaller grain sizes (between 2.0 and 2.7 µm).

Regarding the case of bimodal ($\alpha + \beta$) microstructure, tensile responses of some bimodal microstructures were plotted in Fig. 4(b) (among 9 in total). The influence of the aging process can be observed by comparing Fig. 4(a) and Fig. 4(b). As expected, a greater strength was reached with the addition of aging processes (450°C, 550°C, 650°C) starting from the same annealing conditions (for example 900°C-240 min-AC). Whereas strength is improved in every case, ductility is kept only for prior annealing conditions of 240 min while ductility is slightly deteriorated for the bimodal microstructures having prior annealing times of 30 min and highly deteriorated for the ones of 90 min. The samples having low ductility and high strength correspond to small α grain sizes (around 2.7 µm) and lower α fraction data (around 76% of primary α). In contrast, the microstructures with coarser α grains (4.2 µm) and larger α fraction (around 80%) correspond to the high strength and ductility kept response.

For the duplex ($\alpha + \alpha'$) microstructures, heat treatment temperatures vary from 850°C to 980°C while the holding times are fixed at 15 min, thus allowing fine grains. Therefore, a linear evolution of phase proportion regarding grain size was observed for the 9 duplex microstructures studied. High treatment temperature samples correspond to coarse grain sizes with a large amount of α' martensite formed (fraction of primary α phase is low). An example of their stress-strain curves is shown in Fig. 4(c) (980°C-15 min-STQ) with especially high strength and low work hardening rate. A transition in the mechanical response can be seen when progressively decreasing the treatment temperatures (950°C-15 min-STQ in Fig. 4(c)) where strength properties are decreasing a little while work hardening is improving. More precisely, such improvement in work hardening ability is mainly obtained by diminishing and balancing the amount of α' martensite over primary α phase. Such transition is completed when getting to temperatures between 880°C and 920°C (880°C and 900°C samples are represented in Fig. 4(c)) where work hardening is peaking and strength is only diminished by a little. To be precise, UTS is kept while proof stress is decreasing, thus causing an improvement in work hardening. It is noticeable that such properties are obtained for proportions of α' martensite around 40–50%.

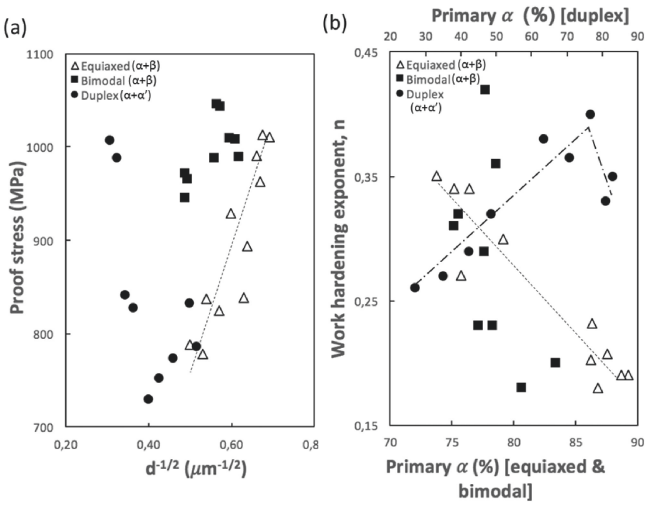

Fig. 5 Effects of (a) grain size on proof stress and (b) primary α fraction on work hardening for the various microstructures.

To summarize the mechanical properties as a function of microstructural factors, Fig. 5 summarizes (a) the proof stress as a function of grain size of primary α phase ($d^{-1/2}(\mu m^{-1/2})$) and (b) the work hardening exponent n as a function of fraction of primary α grain. Here, n is estimated as $\Delta[\log(\sigma_{true})]/\Delta[\log(\varepsilon_{true})]$ for differences Δ taken between proof stress and UTS.

From Fig. 5(a), we can observe a good correlation between proof stress and grain size of primary α phase only for the equiaxed ($\alpha+\beta$) microstructure, implying that strengthening according to Hall-Petch relation is applied only for equiaxed microstructure. On the other hand, there is a stronger scattering for the bimodal ($\alpha+\beta$) and duplex ($\alpha+\alpha'$) duplex microstructures. With respect to the relation between fraction of primary α phase and work hardening exponent n as shown in Fig. 5(b), a good correlation is observed for a decreasing n while increasing primary α fraction. Thus, an increasing the fraction of β phase contributes to the homogeneous deformation due to higher activation of multiple slips in the β phase as compared to the α phase. As for the duplex ($\alpha+\alpha'$) microstructure, it is interestingly noted that the n increases with increasing the fraction of primary α phase up to approximately 85%, followed by a decreasing of work hardening exponent, n. As mentioned for the equiaxed ($\alpha+\beta$) microstructure, the primary α phase does not act as an enhancing factor of the n. Therefore, the increase of n with primary α fraction for the duplex ($\alpha+\alpha'$) microstructure is supposed to be due to the α' martensite and balance of α/α' fraction. On the other hand, from Fig. 5(b), no correlation is observed for the bimodal ($\alpha+\beta$) microstructure, indicating that work hardening behavior (in relation to homogeneous deformation mode) is not simply dominated by the ratio of primary $\alpha/(\alpha+\beta)$ lamellae for the bimodal ($\alpha+\beta$) microstructure.

3.1.3 Strength-ductility balance and dynamic work-hardening behavior

Here, the effects of microstructural factors on the strength-ductility balance and the dynamical change in work hardening behavior with straining are summarized. The equiaxed, bimodal and duplex microstructures investigated in this research are quantitatively compared in Fig. 6. It comes out that the duplex ($\alpha+\alpha'$) microstructures display more attractive properties than the others.

Outstandingly, duplex samples can reach even greater ductility properties (plastic elongation) than equiaxed microstructures, which are known for being ductile. On the other hand, duplex microstructures show excellent strength (UTS) properties which are as high as bimodal ones. The exceptional strength and ductility balance of the duplex ($\alpha+\alpha'$) microstructure can be seen in Fig. 6(a). Nevertheless, its work hardening ability is also surpassing the ones of equiaxed and bimodal microstructures as shown in Fig. 6(b), where the dynamic work hardening rate is plotted. Indeed, the stationary part of the curves (after 0.07 true strain) shows higher and longer plateaus for duplex ($\alpha+\alpha'$) microstructure.

3.1.4 Distributions of geometrically necessary dislocation density

Here, we discuss a higher ductility in the duplex ($\alpha+\alpha'$) microstructure than the bimodal ($\alpha+\beta$) microstructure in terms of strain distribution in a deformed microstructure. Figure 7 summarizes the frequency of local misorientation degrees obtained by EBSD local misorientation maps before and after tensile deformation at a plastic strain of 5% (for (a) bimodal ($\alpha+\beta$) microstructure and (b) duplex ($\alpha+\alpha'$) microstructure) (heat treatments at (a) 900°C-30 min followed by aging at 650°C-120 min, and (b) 950°C-15 min followed by quenching into ice water). Plastic flow behaviors for these specimens are as shown in Fig. 4. Herein, distributions for α and β phases and that for α phase and α' martensite are shown in (a) and (b) respectively. Regarding the duplex ($\alpha+\alpha'$) microstructure consisting of the same HCP phase, 20 areas in each for primary α phase and α' martensite were extracted from the EBSD data, respectively. And the histogram of local misorientation for each phase (as shown in Fig. 7(b)) was obtained by merging these data of 20 areas. Focusing on the change in the mode before and after deformation of each phase, there is a peak shift of a higher degree for all phases, being indicative of strain accumulation by plastic deformation. Comparing these two microstructures, we can interestingly note that a higher shift in the β phase than the primary α phase is observed for the bimodal ($\alpha+\beta$) microstructure. On the other hand, there is no difference in the change of degree of peak shift of both phases for the duplex ($\alpha+\alpha'$) duplex microstructure. This

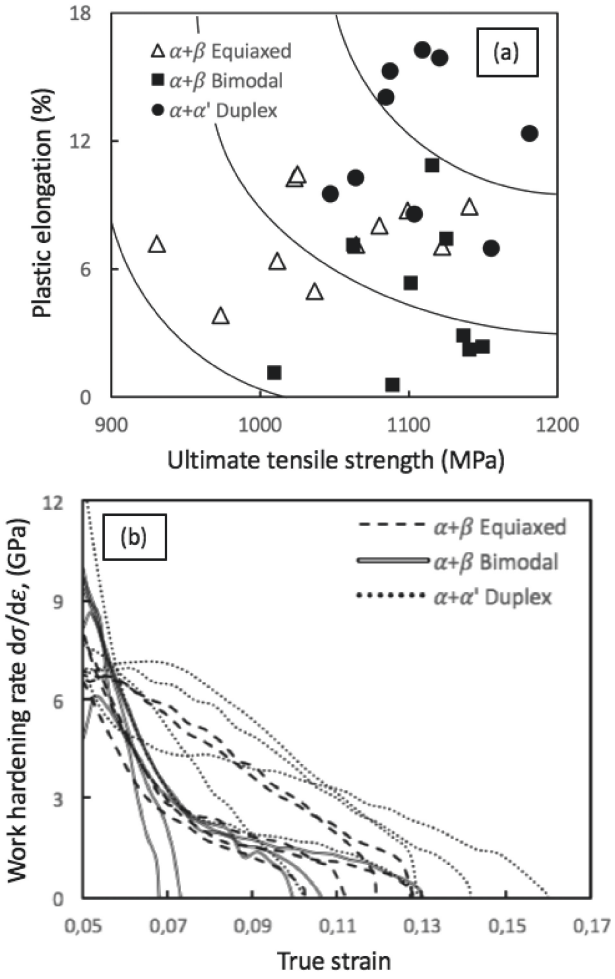

Fig. 6 (a) Plastic elongation – ultimate tensile stress (UTS) balance for different microstructures and (b) Dynamic work hardening rate evolution for different microstructures.

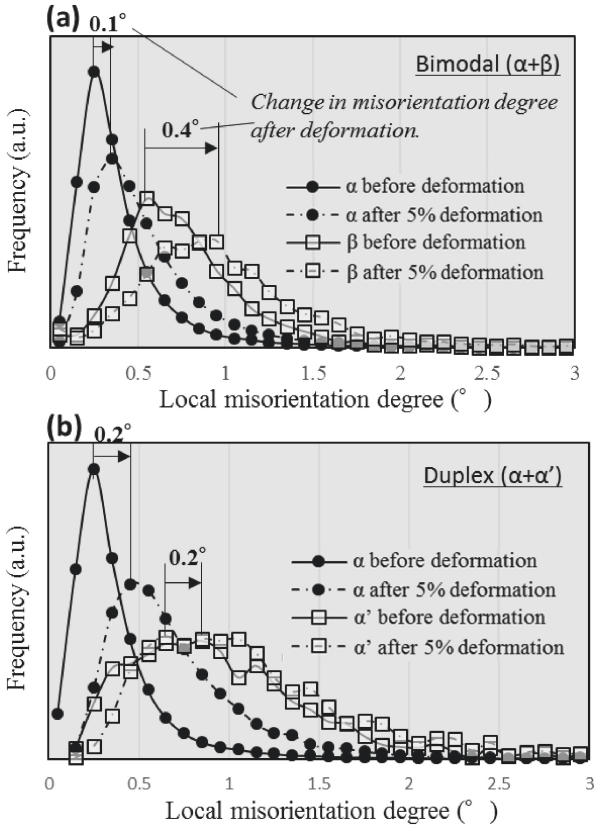

Fig. 7 Distributions of local misorientation estimated by EBSD for (a), (b) the primary α phase and (a) β phase in lamellar ($\alpha + \beta$) region and (b) α' martensite in the duplex ($\alpha + \alpha'$) microstructure of the Ti-6242S alloys before and after tensile deformation at 5% plastic strain. Specimens for (a) 900°C-30 minAC-650°C-120 minOC, (b) 950°C-15 min-STQ.

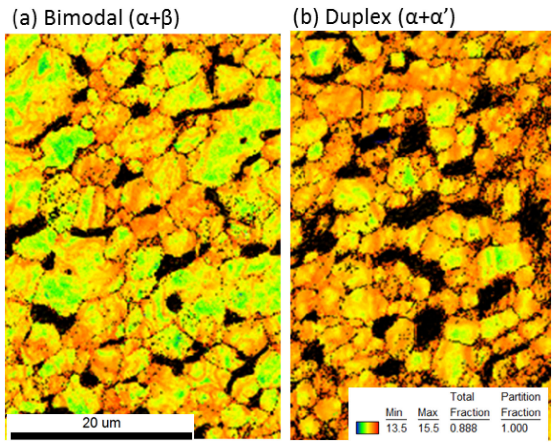

Fig. 8 Distribution of GND density for primary α phase in microstructures after deformation at a plastic strain of 5% of specimens for heat treatment of (a) 900°C-30 min AC-650°C-120 min OQ, (b) 950°C-15 min-STQ.

result implies that homogeneous strain distribution is exhibited in the duplex ($\alpha + \alpha'$) duplex microstructure, resulting in the enhanced homogeneous deformation behavior. Figure 8 shows the distribution of geometrical necessary dislocation (GND) density in the primary α phase (black area corresponds to ($\alpha + \beta$)-lamellae in (a) and α' region in (b), respectively) which is estimated as the following equation. According to Calcagnotto *et al.*, the local misorientation angle assumes a series of cylinder-torsion twist subgrain boundaries, each containing two perpendicular arrays of screw dislocations:[40)]

$$\rho_{gnd} = \frac{2\Delta\theta}{\mu b}$$

where μ is the unit length corresponding to the step size for EBSD analysis ($= 0.15\,\mu m$ in this work) and b is the magnitude of the Burgers vector ($= 2.95 \times 10^{-10}\,m$).

From Fig. 8, we can indeed observe a heterogeneous GND partitioning (composed of highly strain-accumulated grains and grains with less strain) for the bimodal ($\alpha + \beta$) microstructure and a homogeneous one for the duplex ($\alpha + \alpha'$) microstructure. Thus, we can suppose that the acicular α' martensite acts as a homogeneous accommodation site for strain partitioning. Therefore, it leads to the homogenous continuity of straining between the primary α phase and the α' martensite. In this regard, a further direction of this study will clarify the role of α' martensite on local deformation mode around boundaries to figure out the origin of high work hardening and homogeneous deformation more clearly.

Thus, to summarize tensile properties, we should emphasize from the experimental results that the α' martensite in the duplex ($\alpha + \alpha'$) microstructure indeed improves the work hardening behavior, leading to homogeneous deformation and large ductility. Here, we found from Fig. 5 that optimization in fraction of α/α' should be required for the enhanced work hardening (herein, we can note that the fraction of around 85% of primary α phase is an optimum one for the enhanced work hardening exponent most.). As we introduced in the above *1. Introduction*, twinning on $\{10\bar{1}1\}$ or $\{13\bar{4}1\}$ in the α' martensite should play an important role in the enhanced work hardening rate.[10,19)] In this regard, Dumas *et al.*, emphasized that three variants cluster with inter variant consisting of $\{13\bar{4}1\}$ twins were required for the high work hardening rate. So, we can speculate that reorientation of α'-martensite variants associated with $\{13\bar{4}1\}$ twinning is optimally activated for the primary α fraction around 85%, which is thanks to the abovementioned three variants cluster formation in the duplex ($\alpha + \alpha'$) microstructure (as shown in Fig. 5(b)). In general, there are 12 variants formed in the α' martensite, therefore, microstructural control with variant selection (with inter variant consisting of $\{13\bar{4}1\}$) should be required for high work hardening behavior, which should be linked with the result of Fig. 5(b). Further work in this research would clarify it in order to enhance homogeneous deformation mode more and more in a Ti-6242S alloy.

3.2 Quantitative linkage between microstructural factors and tensile properties according to machine learning

3.2.1 Parameter importances

The architecture of a gradient boosting regression tree used in this work is shown in Fig. 9(a). The results are displayed in Fig. 9(b), where the feature importances of each microstructural factor are compared. Herein, we considered typical three microstructural factors of the morphology (equiaxed, bimodal or α-α' duplex), α proportion (fraction of primary α phase) and average grain size of primary α grains. Regarding the factor of fraction of primary α phase, it conversely

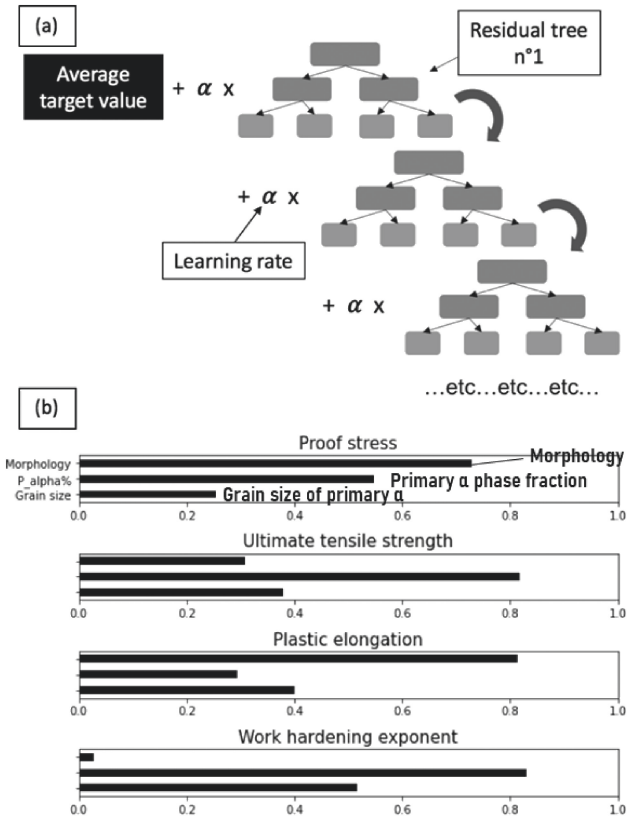

Fig. 9 (a) Gradient boosting regression tree diagram, (b) Feature importance results of the microstructural parameters.

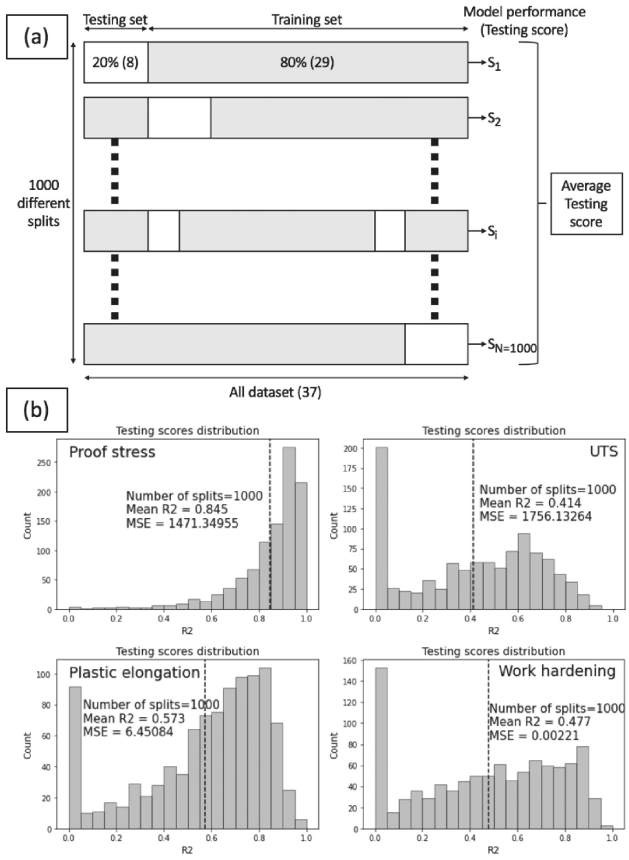

Fig. 10 (a) Cross-validation scheme, (b) Testing scores distributions for the different mechanical properties.

corresponds to fractions of β in equiaxed microstructure, $(\alpha + \beta)$ lamellae in bimodal microstructure and α' martensite in duplex microstructure.

It is important to note that the direct lecture of the results is how each parameter is important for the model itself to predict correctly the outputs. As a consequence, it shows how sensitive the model is regarding each parameter.

It comes out that the kind of microstructures (morphology factor) has the most importance in modeling plastic elongation where primary α fraction and grain size are not influencing much. It coincides with the bad correlation results on the experimental observations done on the 3 microstructures (equiaxed, bimodal, duplex). Therefore, it is coherent that only the morphology parameter is meaningful. For the proof stress, both morphology and α fraction are important for controlling. However, we unintuitively see that grain size importance is very small. It is believed the correlations regarding the Hall-Petch relationship, mainly verified for the equiaxed microstructures (not proven for bimodal and duplex microstructures), have been shifted from the grain size parameter to the morphology parameter. Therefore the morphology has been given more importance than the grain size towards the prediction of proof stress. For the UTS, the α proportion is the most important factor to control which coincides with the excellent experimental correlations obtained for the equiaxed and duplex microstructures. In the model, grain size is twice less important than α proportion but it does not mean its effects are negligible. Finally, both α proportion and grain size are important to model work hardening with a preference with α fraction. Intuitively, the α proportion importance should dominate more the effects of grain size but the linear dependence, experimentally observed between the two factors (especially for the duplex microstructures), manages to maybe overestimate the grain size importance in the model. Thus, the machine learning approach allows us to link the microstructural factor and mechanical properties more reliably, thereby, providing us with quantitative information on their correlation.

3.2.2 Cross-validation

In order to validate the models, data were split into 80% for training the models and 20% for testing them. Because the dataset is pretty small, the results were very dependent on the split considered. Therefore, a user-defined method of cross-validation (close to the Leave-P-Out cross-validation method) using a total of 1000 different possible splits was used (Fig. 10(a)). Average testing scores (coefficient of determination R^2) of 0.85, 0.57, 0.48 and 0.41 were found respectively for proof stress, plastic elongation, work hardening and UTS models. The repartitions of the testing scores (R^2) can be seen in Fig. 10(b).

Furthermore, square roots of the MSE (mean squared errors) give a complementary response for the validity of the models. Errors of 38.3 (MPa), 41.9 (MPa), 2.54 (%) and 0.047 (−) were found respectively for proof stress, UTS, plastic elongation and work hardening (exponent). Thus corresponding respectively to relative errors of 4.26%, 3.85%, 28.5% and 16.0% when predicting target values using data unseen by the model (testing data). Assessing if

the model is a good fit or not is a complicated task to do. By looking at both metrics (R^2 and MSE), we can judge that the proof stress model is certainly trustworthy. However, the validation of the other models is still ambiguous. In order to improve both the models themselves and their level of trust, it would be suitable to improve the size of the dataset, by increasing the number of samples or the number of microstructural features for example.

Hopefully, the average feature importances from each different test split were extremely similar to the importance results obtained from using the whole dataset. Thus allowing us to consider the feature importances as decent results even though the testing validation was sometimes not enough to fully trust the models (mainly because the dataset is too small). Essentially, machine learning with the gradient boosting regression tree algorithm allows getting a complementary approach on how the microstructural parameters (grain size and α proportion) control the mechanical properties (proof stress, UTS, plastic elongation, work hardening). Because grain size and α proportion both contribute to the mechanical properties, it is difficult to quantify their effects only through experimental results whereas machine learning algorithms can model it more easily.

4. Conclusion

The equiaxed ($\alpha + \beta$), bimodal ($\alpha + \beta$) and duplex ($\alpha + \alpha'$) microstructures of a Ti–6Al–2Sn–4Zr–2Mo–Si (Ti-6242S) titanium alloy were characterized. In this work, microstructural factors such as the grain size, morphology and fraction of α/β or α/α' were variously changed by controlling the static heat treatment conditions. The corresponding tensile properties (strength, ductility and work hardening behavior) were evaluated. Regarding the duplex ($\alpha + \alpha'$) microstructure for example, the influence of the treatment duration was investigated. The decrease of solution treated temperature would reduce the grain size and the amount of α' martensite produced (i.e. increase the primary α fraction).

As for tensile properties in relation to microstructural factors, the correlations for the equiaxed microstructure showed that strength could be easily controlled thanks to grain size (Hall-Petch law) and that β phase could control work hardening. The equiaxed microstructures were found to be especially ductile (high plastic elongation) with good work hardening while strength was average compared to bimodal ($\alpha + \beta$) and duplex ($\alpha + \alpha'$) microstructures. On the other hand, high strength (but with low work hardening rate) is exhibited in the case of the bimodal ($\alpha + \beta$) microstructure. Herein, the study of correlations could not precisely point out the influence of the microstructural factors on the mechanical properties. Regarding the duplex ($\alpha + \alpha'$) microstructure, it showed great control of strength and work hardening thanks to the amount of α' martensite formed. Moreover, the balance between strength and work hardening is surprisingly interesting, reaching high work hardening and good strength. Nonetheless, the ductility of the duplex microstructure is also very good overall.

The three microstructures were then compared, highlighting the advantages of the $\alpha + \alpha'$ duplex microstructure regarding its superior work hardening and strength-ductility balance.

Finally, a complementary numerical approach was done in order to quantify the effects of the microstructural factors on the mechanical properties. The machine learning model using the gradient boosting regression tree algorithm allowed us to evaluate the importance of the morphology (the type of microstructure), grain size and phase proportion for each mechanical property (proof stress, UTS, plastic elongation and work hardening). The feature importances were analyzed and compared with the experimental observation in order to give an additional understanding of the mechanical control of the Ti-6242S alloy. The validity of the numerical results was investigated thanks to cross-validation showing that the model for proof stress could be trusted whereas additional data was required to improve the trust of the plastic elongation, work hardening and UTS models.

Acknowledgment

This work was financially supported in part by a Grant-in-Aid for Scientific Research from the Light Metals Educational Foundation, Inc., Japan.

REFERENCES

1) G. Lütjering, J.C. Williams and A. Gysler: Microstructure and Mechanical Properties of Titanium Alloys, *Microstructure and Properties of Materials*, ed. by J.C.M. Li, (World Scientific, Singapore, 2000) pp. 1–77.
2) P. Pushp, S.M. Dasharath and C. Arati: Mater. Today: Proc. **54** (2022) 537–542.
3) M. Peters, J. Hemptenmacher, J. Kumpfert and C. Leyens: Structure and Properties of Titanium and Titanium Alloys, *Titanium and Titanium Alloys: Fundamentals and Applications*, ed. by C. Leyens and M. Peters, (Wiley-VCH, Weinheim, 2003) pp. 1–36.
4) M.T. Jia, D.L. Zhang, B. Gabbitas, J.M. Liang and C. Kong: Scr. Mater. **107** (2015) 10–13.
5) X.P. Ren, H.Q. Li, H. Guo, F.L. Shen, C.X. Qin, E.T. Zhao and X.Y. Fang: Mater. Sci. Eng. A **817** (2021) 141384.
6) Y. Chong, T. Bhattacharjee, J. Yi, S. Zhao and N. Tsuji: Materialia **8** (2019) 100479.
7) R.R. Boyer: Mater. Sci. Eng. A **213** (1996) 103–114.
8) R.K. Gupta, C. Mathew and P. Ramkumar: Frontiers in Aerospace Engineering **4**(1) (2015) 1–13.
9) Y. Chong, G. Deng, J. Yi, A. Shibata and N. Tsuji: J. Alloy. Compd. **811** (2019) 152040.
10) O. Dumas, L. Malet, B. Hary, F. Prima and S. Godet: Acta Mater. **205** (2021) 116530.
11) Q. Zhao, L. Bolzoni, Y. Chen, Y. Xu, R. Torrens and F. Yang: J. Mater. Sci. Technol. **126** (2022) 22–43.
12) J. Wang, W. Xiao, Y. Fu, L. Ren and C. Ma: Prog. Nat. Sci.: Mater. Int. **32** (2022) 63–71.
13) Z. Wang, L. Liu, L. Zhang, J. Sheng, D. Wu and M. Yuan: Mater. Trans. **60** (2019) 269–276.
14) Z.W. Huang, P.L. Yong, H. Zhou and Y.S. Li: Mater. Sci. Eng. A **773** (2020) 138721.
15) Y. Chong, G. Deng, S. Gao, J. Yi, A. Shibata and N. Tsuji: Scr. Mater. **172** (2019) 77–82.
16) J.Y. Jung, J.K. Park, C.H. Chun and S.M. Her: Mater. Sci. Eng. A **220** (1996) 185–190.
17) H. Takebe and K. Ushioda: Mater. Trans. **62** (2021) 952–961.
18) H. Matsumoto, D. Tadokoro and I. Séchepée: ISIJ Int. **61** (2021) 2844–2854.
19) S. Cao, R. Chu, X. Zhou, K. Yang, Q. Jia, C.V.S. Lim, A. Huang and X. Wu: J. Alloy. Compd. **744** (2018) 357–363.
20) J. Su, X. Ji, J. Liu, J. Teng, F. Jiang, D. Fu and H. Zhang: J. Mater. Sci.

Technol. **107** (2022) 136–148.
21) H. Matsumoto, H. Yoneda, K. Sato, S. Kurosu, E. Maire, D. Fabregue, T.J. Konno and A. Chiba: Mater. Sci. Eng. A **528** (2011) 1512–1520.
22) T. Morita, K. Hatsuoka, T. Iizuka and K. Kawasaki: Mater. Trans. **46** (2005) 1681–1686.
23) C. de Formanoir, G. Martin, F. Prima, S.Y.P. Allain, T. Dessolier, F. Sun, S. Vivès, B. Hary, Y. Bréchet and S. Godet: Acta Mater. **162** (2019) 149–162.
24) T. Shiraiwa, Y. Miyazawa and M. Enoki: Mater. Trans. **60** (2018) 189–198.
25) J. Syarif, Y.P. Detak and R. Ramli: ISIJ Int. **50** (2010) 1689–1694.
26) S. Guo, J. Yu, X. Liu, C. Wang and Q. Jiang: Comput. Mater. Sci. **160** (2019) 95–104.
27) S. Malinov, W. Sha and J.J. McKeown: Comput. Mater. Sci. **21** (2001) 375–394.
28) J.S. Suh, B.-C. Suh, S.E. Lee, J.H. Bae and B.G. Moon: J. Mater. Sci. Technol. **107** (2022) 52–63.
29) C. Dumortier and P. Lehert: ISIJ Int. **39** (1999) 980–985.
30) C. McElfresh, C. Roberts, S. He, S. Prikhodko and J. Marian: Comput. Mater. Sci. **208** (2022) 111267.
31) Z.-L. Wang, T. Ogawa and Y. Adachi: ISIJ Int. **59** (2019) 1691–1694.
32) I.S. Markham and T.R. Rakes: Computers Ops Res. **25** (1998) 251–263.
33) Y. Zhang and A. Haghani: Transp. Res., Part C Emerg. Technol. **58** (2015) 308–324.
34) P. Körner, R. Kronenberg, S. Genzel and C. Bernhofer: Meteorologische Zeitschrift **27** (2018) 369–376.
35) A. Altmann, L. Toloşi, O. Sander and T. Lengauer: Bioinformatics **26** (2010) 1340–1347.
36) J.S. Jha, S.P. Toppo, R. Singh, A. Tewari and S.K. Mishra: Mater. Charact. **171** (2021) 110780.
37) Y. Zhang, S. Fang, Y. Wang and D. Zhang: Mater. Sci. Eng. A **803** (2021) 140701.
38) S. Sun, D. Zhang, S. Palanisamy, Q. Liu and M.S. Dargusch: Mater. Sci. Eng. A **839** (2022) 142817.
39) J.C. Williams, R. Tagart and D.H. Polonis: Metall. Trans. **1** (1970) 2265–2270.
40) M. Calcagnotto, D. Ponge, E. Demir and D. Raabe: Mater. Sci. Eng. A **527** (2010) 2738–2746.